Nonhyperbolic behavior in the thermostated Lorentz gas

H. Odbadrakh and G. P. Morriss
School of Physics, University of New South Wales, Sydney, New South Wales 2052, Australia
(Received 23 March 1999; revised manuscript received 18 June 1999)

We show that nonhyperbolic behavior in the length-2 periodic orbits of the thermostated random Lorentz gas occurs only at field strengths greater than unity. For the thermostatted periodic Lorentz gas the range of fields is reduced further due to pruning. Stability analysis shows that there are three classes of period-2 orbits: elliptic orbits and two different hyperbolic orbits. Within the nonergodic elliptic region, trajectories manifest complex behavior that resembles that of perturbed resonant tori in Hamiltonian systems. We present a detailed dynamical study of the nonhyperbolic region. [S1063-651X(99)14410-6]

PACS number(s): 05.45.−a, 05.70.Ln

I. INTRODUCTION

The thermostated periodic Lorentz gas [1–8] has been studied extensively as a model for nonequilibrium steady states [4,9–12]. For the most frequently studied state and applied fields ϵ in the range $0 \leqslant \epsilon \leqslant 2.2$, the phase space is ergodic. At larger values of ϵ, the attractor is at first a fractal with dimension smaller than the phase space, and then the attractor separates into two disjoint components: one an ergodic chaotic fractal and the other a stable elliptic region. The emergence of the stable elliptic region signals the breakdown of ergodic behavior in the thermostated periodic Lorentz gas [13]. A complicated region then follows that includes both chaotic components and stable periodic orbits, often appearing together at the same value of ϵ. Finally the complicated region gives way to stable periodic orbits that eventually end with a simple period-2 orbit. Increasing the value of ϵ still further introduces multiple bounces on the same scatterer, with the high field limit being a creeping orbit that follows the curvature of each scatterer until it falls to the next scatterer. The creeping trajectory is made up of infinitely many bounces on each scatterer along a channel (if the direction of the channel and the field are similar).

The thermostated random Lorentz gas has been proposed as a more realistic model of high dimensional nonequilibrium steady states as it removes (or at least minimizes) the effects of periodicity. The Lyapunov spectrum has been calculated using both kinetic theory [14,15] and numerical simulation [16], and the results are in excellent agreement. However, it has been suggested that between particular pairs of scatterers in the random Lorentz gas, there could exist small elliptic regions that are disjoint nonergodic components [17] and that these may be present at all nonzero values of the field. The existence of such regions would imply that the thermostated random Lorentz gas is not ergodic. In this paper we explore this possibility by studying periodic orbits between individual pairs of scatterers as a function of separation and orientation, assuming a cavity sufficiently large enough to contain the orbit. The probability of finding a cavity is inversely proportional to the size, so that cavities of all sizes are possible.

The Lorentz gas has also been used to construct mappings that contain many of the same physical features but are easier to analyze mathematically [18]. The major advantage of these maps is that the expanding and contracting directions are aligned with the two coordinate axes everywhere in the phase space. The global bifurcation behavior of these maps is similar to, but less complicated than, the original Lorentz gas. In particular, the elliptic region that we study here is absent from the map.

II. THERMOSTATED LORENTZ GAS

A. The model

In the periodic Lorentz gas the wandering particle experiences the combined effects of an external field and a thermostat as it moves and scatters from a hexagonal lattice of hard disk scatterers. The equations of motion with an external field ϵ in the x direction and an isokinetic thermostat are given by [3]

$$\dot{x} = p_x, \quad \dot{p}_x = F_x - \epsilon - \alpha p_x,$$
$$\dot{y} = p_y, \quad \dot{p}_y = F_y - \alpha p_y \tag{1}$$

where $\alpha = -\epsilon p_x / p^2$. The presence of the thermostat ensures that the particle speed must be constant. For simplicity, we take the speed p of the particle and its mass to be unity. Integrating the equations of motion in polar coordinates, we can find the time evolution of the coordinates and the direction of the momentum:

$$x_1 - x_0 = \frac{1}{\epsilon} \ln \frac{\sin \theta_1}{\sin \theta_0}, \tag{2}$$

$$y_1 - y_0 = \frac{1}{\epsilon} (\theta_1 - \theta_0), \tag{3}$$

$$\tan\left(\frac{\theta_1}{2}\right) = \tan\left(\frac{\theta_0}{2}\right) \exp[\epsilon (t_1 - t_0)], \tag{4}$$

where x_0 and y_0 are the initial coordinates of the particle, θ_0 is the initial direction of the momentum, and t_0 is the initial time. These equations give values of x_1, y_1, and θ_1 at any time t_1, after the initial time.

The geometry of a collision can be described by specifying the point on the surface of the scatterer where the collision takes place, and the angle of the momentum vector be-

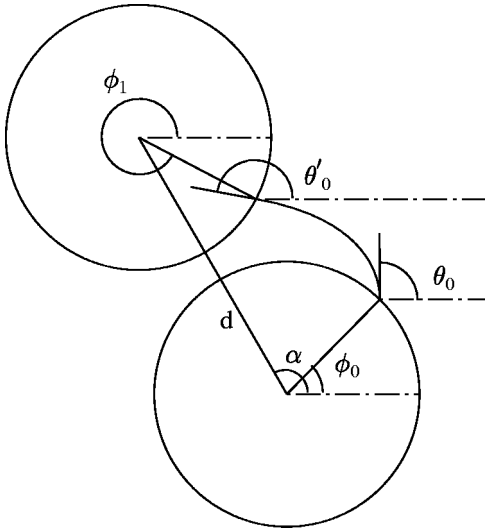

FIG. 1. Geometry of a free flight between two scatterers. θ_0 and ϕ_0 are initial coordinates in the Poincaré section and θ'_0 and ϕ_1 are the coordinates before the next collision. d is the distance between centers of the two scatterers and α is the angle between the line joining the centers and the x axis.

fore collision (both angles are measured relative to the x axis). We take these angles as coordinates in a Poincaré surface of section. So, if the coordinates after one collision are (θ_0,ϕ_0), then the coordinates before the next collision are (θ'_0,ϕ_1), and these are related by the equations

$$\sin\phi_0+\frac{1}{\epsilon}(\theta'_0-\theta_0)-\sin\phi_1=d\sin\alpha_0,$$

$$\cos\phi_0+\frac{1}{\epsilon}\ln\left(\frac{\sin\theta'_0}{\sin\theta_0}\right)-\cos\phi_1=d\cos\alpha_0, \tag{5}$$

where d is the distance between the centers of the two hard disk scatterers and α_0 is the angle between the x axis and the line connecting the center of scatterer 0 to scatterer 1 (see Fig. 1). Here we take the radius of the disks as unity. In the collision ϕ is unchanged, but $\theta_1=2\phi-\theta'_0\pm\pi$.

For the periodic Lorentz gas it is usual to define a symbolic dynamics that reduces the level of description of a generic trajectory to a list of symbols, each one representing a single free flight between two scatterers [3]. The symbol that is attached to a free flight is determined uniquely by the relative separation of the two scatterers [that is, the vector from the center of the first scatterer to the center of the second (Fig. 2)]. Therefore, a finite length of trajectory has a unique symbol sequence. Moreover, the phase space of the Lorentz gas can be partitioned into regions, which contain all the initial conditions that follow a particular symbol sequence. This is summarized in Sec. III A.

B. Stability

We consider the stability of the first return mapping M, which consists of two free flights and two collisions. In the notation we have used, this mapping is $(\theta_2,\phi_2)=M(\theta_0,\phi_0)$ and $\theta_2=\theta_0$, and $\phi_2=\phi_0$ constitutes a periodic orbit of length 2. The stability matrix for the collision is

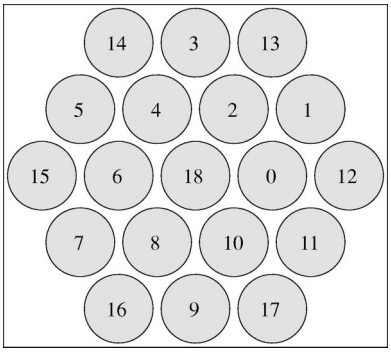

FIG. 2. Symbolic representation of the dynamics for the periodic Lorentz gas. The central disk labeled 18 is the initial scatterer. The label attached to the free flight is the label on the final scatterer. For example, the (0-6) trajectory begins from 18 and then collides with 0, then the origin (scatterer 18 moves to the old position of 0), and the wandering particle moves to the left to collide with scatterer 6.

$$J_C=\begin{pmatrix}-1 & 2\\ 0 & 1\end{pmatrix}, \tag{6}$$

and the free flight from (θ_0,ϕ_0) to (θ'_0,ϕ_1) is [3]

$$J_f(1,0)=\begin{pmatrix}\dfrac{\sin\theta'_0\cos(\phi_1-\theta_0)}{\sin\theta_0\cos(\phi_1-\theta'_0)} & \dfrac{-\epsilon\sin\theta'_0\sin(\phi_1-\phi_0)}{\cos(\phi_0-\theta'_0)}\\ \dfrac{\sin(\theta'_0-\theta_0)}{\epsilon\sin\theta_0\cos(\phi_1-\theta'_0)} & \dfrac{\cos(\phi_0-\theta'_0)}{\cos(\phi_0-\theta'_0)}\end{pmatrix}. \tag{7}$$

The stability matrix (or the Jacobian) for the map M is the product of four of these matrices $[J_CJ_f(2,1)J_CJ_f(1,0)]$ and is a function of the initial coordinates (θ_0,ϕ_0). For periodic points of the map, the real part of the logarithms of the eigenvalues of the Jacobian gives the Lyapunov exponent λ times the period τ. For quasiperiodic trajectories, it is necessary to consider multiple applications of the map, and take the long time limit, to obtain the Lyapunov exponents [19]. The periodic $(4-10)$ orbit has normal collisions with each scatterer, so that $\theta_0=\phi_0,\theta_1=\phi_1$ and $\theta_1-\theta'_0=-\pi,\theta_2-\theta'_1=\theta_0-\theta'_1=-\pi$. So Eq. (7) becomes

$$J_f(1,0)=\begin{pmatrix}\dfrac{\sin\theta'_0\cos(\theta'_0-\theta_0)}{\sin\theta_0} & -\epsilon\sin\theta'_0\sin(\theta'_0-\theta_0)\\ \dfrac{-\sin(\theta'_0-\theta_0)}{\epsilon\sin\theta_0} & -\cos(\theta'_0-\theta_0)\end{pmatrix}. \tag{8}$$

Calculating the eigenvalues Λ_i of the Jacobian of the mapping for each periodic orbit gives the Lyapunov exponents $\lambda_i=(1/\tau)\mathrm{Re}\{\ln(\Lambda_i)\}$ and enables us to identify the stability of the orbit. In general, the eigenvalues can be either real or complex. If the eigenvalue equation is $J\mathbf{e}=\Lambda\mathbf{e}$, then a negative eigenvalue implies that the direction of the eigenvector

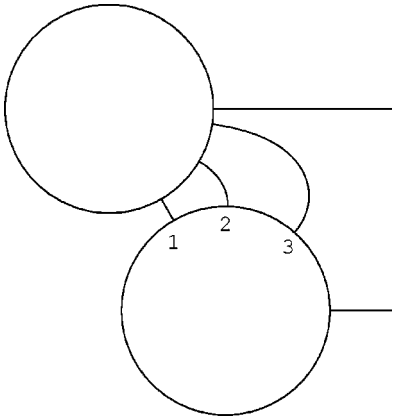

FIG. 3. Full range of possible periodic orbits for $\alpha=2\pi/3$ and $d=2.236$ as a function of ϵ. The orbit marked (1) is the $\epsilon=0$ orbit; the orbit marked (2) is the limiting hyperbolic orbit at $\epsilon=2.464$; the the orbit marked (3) is the limit for the elliptic orbit at $\epsilon=2.066$. The two horizontal lines represent the limiting orbit at $\epsilon=1.623$. Any orbit between (1) and (2) is hyperbolic and any orbit between (2) and (3) is elliptic. Any orbit between (3) and the horizontal lines has real negative eigenvalues, but has one positive Lyapunov exponent, so is hyperbolic.

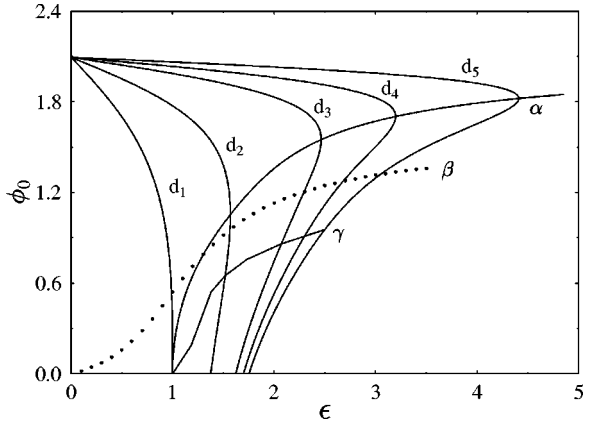

FIG. 4. Field dependence of the initial conditions for periodic orbits for $\alpha=2\pi/3$, at different separation lengths d. The curve labeled d_1 gives the initial ϕ value as a function of field for $d_1=3.6276$. Other curves correspond to $d_2=2.9318$, $d_3=2.236$, $d_4=2.143$, and $d_5=2.05$. d_1 is the maximum possible distance for the existence of the elliptic region between the two scatterers. The curve α is the border between hyperbolic and elliptic periodic orbits, the dashed curve β is the pruning caused by disk 2 for the periodic Lorentz gas, and the curve γ is border between elliptic and the return of hyperbolic orbits.

is reversed by the mapping, whereas there is no reversal for a positive eigenvalue. An orbit for which at least one of the Lyapunov exponents is positive is termed an unstable orbit. If all the Lyapunov exponents are negative the orbit is stable, but if all the Lyapunov exponents are equal to zero the orbit is neutrally stable. For a two-dimensional phase space, a periodic orbit with one positive and one negative Lyapunov exponent is a hyperbolic point. If both Lyapunov exponents are equal to zero then the orbit is elliptic.

III. PERIODIC ORBITS BETWEEN TWO SCATTERERS

It is more revealing to study the periodic orbits between two arbitrarily placed scatterers in isolation. In this way we can investigate periodic orbits without considering the effects of pruning by other scatterers. For a given field, the maximum vertical displacement in a trajectory between two scatterers is given by π/ϵ [20]. For two scatterers separated vertically, this trajectory consists of a horizontal flight from the current x to $+\infty$, a vertical flight of π/ϵ at $+\infty$, and the return from $+\infty$ to the new x value (Fig. 3).

Equations (5) can be used to find the initial conditions for periodic orbits of length 2 between two disks with fixed separation d and orientation α. Such orbits have normal collisions with each scatterer so that $\phi_0=\theta_0$ and $\phi_1=\theta_0'-\pi$. Equations (5) then become

$$\epsilon(d\sin\alpha_0-\sin\theta_0-\sin\theta_0')=\theta_0'-\theta_0,$$
$$\exp[\epsilon(d\cos\alpha_0-\cos\theta_0-\cos\theta_0')]=\frac{\sin\theta_0'}{\sin\theta_0}. \tag{9}$$

These equations can be solved to find θ_0 and θ_0'. Here we consider $\alpha_0=2\pi/3$, which for the periodic Lorentz gas corresponds to (4-10) orbits.

For small separation and external field, there is only one solution of Eqs. (9) that represents a hyperbolic periodic orbit. For high enough field, two different solutions exist. Increasing the field further, the two solutions coalesce and disappear, and no (4-10) periodic orbits exist. For very small separations, the two orbits exist up to quite large fields. This analysis is correct for small separations, but when the separation is greater than 3.6276, there is again only one solution corresponding to a hyperbolic orbit. This indicates that a second solution is possible only for scatterers that are close enough.

All of these features are presented in Fig. 4. Curves d_i correspond to solutions of Eqs. (9) for different separations with $d_i>d_{i+1}$, and for fixed α. The boundary between hyperbolic and elliptic orbits is represented by curve α, which consists of the solutions of the equation $\partial\epsilon(\phi_0)/\partial\phi_0=0$ for different separations. If there exists a solution for any d, then this is a peak of the function $\epsilon(\phi_0)$. This implies that there must be a certain range of ϵ that corresponds to two different values of ϕ_0. Therefore, the curves d_i are divided into two parts by the curve α. The upper part consists of hyperbolic orbits, while the lower part consists initially of elliptic orbits. The curve $d_1=3.6276$ is the limiting case, to the left of which all solutions will be hyperbolic. In the periodic Lorentz gas, the pruning of trajectories by neighboring disks is inevitable. Therefore, the dashed curve β corresponds to the pruning caused by disk 2.

If the scatterer that causes the pruning is removed, we find that there is a transition from elliptic to hyperbolic orbits at the curve labeled γ in Fig. 4. Below the curve γ the orbit again becomes hyperbolic. The linear stability analysis reveals that the curve γ is the border between complex eigenvalues and real negative eigenvalues. In the elliptic region, where the eigenvalues are complex, the modulii of the eigenvalues are equal to 1, so the Lyapunov exponents are both zero. The complexity of the eigenvalues implies that the initial state vectors are rotated with each mapping, leading to complex phase space structure within the elliptic region. De-

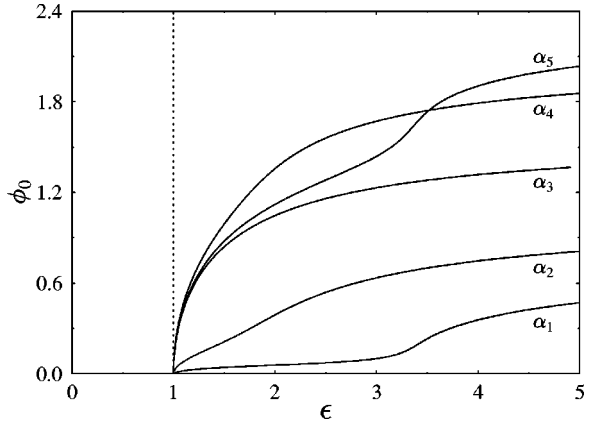

FIG. 5. Border between hyperbolic and elliptic orbits at different relative orientations of the scatterers $\alpha_1=\pi/4$, $\alpha_2=\pi/3$, $\alpha_3=\pi/2$, $\alpha_4=2\pi/3$, and $\alpha_5=3\pi/4$. The curve labeled α_4 is the curve labeled α in Fig. (3). The maximum separation lengths corresponding to each angle are $d_1=d_5=4.44$, $d_2=d_4=3.6276$, and $d_3=3.141\,59$. For all cases the two solutions emerge from the point $\epsilon=1.0$, $\phi_0=0$. The maximum separation length for $\alpha=\pi/2$ is $d_3=\pi$ (where $\epsilon=1.0$), which is the maximum vertical displacement.

tails of this will be discussed in the Sec. III B.

We study the existence of two solutions for different orientations of scatterers. In Fig. 5 we display the curve α for different orientation angles $\alpha_1=\pi/4$, $\alpha_2=\pi/3$, $\alpha_3=\pi/2$, $\alpha_4=2\pi/3$, and $\alpha_5=3\pi/4$. Maximum separations of the two scatterers are given by $d_i^{max}=\pi/\epsilon\cos(\alpha_i-\pi/2)$ so that $d_1=d_5=4.44$, $d_2=d_4=3.6276$, and $d_3=3.141\,59$. For all cases the two solutions emerge at the point $\epsilon=1.0,\phi_0=0$. When the external field is normal to the orientation of the two disks, $\alpha=\pi/2$, the maximum separation length is equal to the maximum vertical displacement of the wandering particle. Thus, $d_3=\pi$ when $\epsilon=1.0$. Furthermore, the linear stability analysis reveals more details on the structure of the phase space.

A. Partitions of the phase space

For the periodic Lorentz gas, the symbolic dynamics allows us to express any path of the wandering particle by a sequence of symbols. This means that we can partition the phase space into regions for which trajectories follow the same sequence of symbols [21]. For the periodic Lorentz gas, it can be done effectively by taking the collision coordinates as phase space variables. We consider partitioning the phase space into regions for which each initial condition begins with the same two symbols.

First we consider the partitioning for one symbol. In order to collide with a particular scatterer the wandering particle must hit that scatterer with a certain value of θ_0'. The maximum and minimum values of θ_0' correspond to the trajectories that are tangent to the two sides of the scatterer, so that $\phi_1\perp\theta_0'$ or $|\phi_1-\theta_0'|=\pi/2$. So Eqs. (5) can then be rewritten as

$$\epsilon(d\sin\alpha_0-\sin\phi_0\pm\cos\theta_0')=\theta_0'-\theta_0,$$

$$\exp[\epsilon(d\cos\alpha_0-\cos\phi_0\mp\sin\theta_0')]=\frac{\sin\theta_0'}{\sin\theta_0}. \qquad (10)$$

Solving Eqs. (10) for a particular disk, a set of limiting values of (θ_0,ϕ_0) can be found. Each pair of (θ_0,ϕ_0) in the set is the initial condition for the corresponding tangent orbit. However, thanks to symmetry properties of the Lorentz gas, we need only a few such sets to partition the phase space. Indeed, the sets corresponding to the maximum value of θ_0' for disks 0, 2, 4, and 6 can be used as sets for the minimum value of θ_0' for disks 0, 10, 8, and 6. We use here the transformation $(\theta_0,\phi_0)\rightarrow(-\theta_0,-\phi_0)$. For high enough field, the combined effects of an external field and a thermostat exclude the existence of the tangent trajectories corresponding to the minimum values of θ_0' for disks 2 and 4. According to the transformation, they could be the sets for the maximum values of θ_0' for disks 8 and 10. The previous sets can again be used to partition the phase space for the second symbol. Time reversibility of the system will play a role in this case [21]. The time reversal is equivalent to the transformation $(\theta_0,\phi_0)\rightarrow(\theta_0+\pi,\phi_0+\pi)$ so that the partitioning for the first symbol can be transformed into the partitioning for the second symbol. Embedding the two pictures in the phase plane, we obtain the phase space partitioning for two symbols. The partitioning of the phase space is illustrated in Fig. 6. For those partition elements that are hyperbolic, a single unstable periodic point exists in each region. The hyperbolic regions (4-10) and (2-8) [and the symmetry related (8-2) and (10-4)] may also contain a single elliptic fixed point. This elliptic fixed point is associated with the nonergodic elliptic region. The unstable periodic point of the (4-10) region is labeled as u and the elliptic fixed point is the center of the elliptic region. For $\epsilon=2.35$ the elliptic fixed point is within the $(4-10)$ partition, so is physically realizable, whereas for $\epsilon=2.25$ the elliptic fixed point is pruned by scatterer number 2. As shown in Fig. 4, for a certain range of fields there will be no elliptic region in the phase space but an unstable fixed point with negative eigenvalues. The structure of the non-ergodic elliptic region will be discussed in more detail in the next subsection.

B. Structure of the elliptic region

The mapping $(\theta_2,\phi_2)=M(\theta_0,\phi_0)$ represents the continuous time dynamics of the Lorentz gas on a surface of section. We take this surface as the phase plane and the collision coordinates as phase variables. The phase portrait of the Lorentz gas for periodic orbits of length 2 reveals interesting properties of the dynamics. We concentrate on the elliptic region, in which the eigenvalues of the stability matrix are complex and the ergodicity of the system breaks down. The center of the elliptic region is the elliptic period-2 orbit, which is a single point in phase space. Apart from the center, a sufficient number of mappings of an initial condition all lie on a closed curve. This indicates the existence of a constraint surface associated with the elliptic orbits in the complete phase space. Further departure from the center results in a splitting of the closed curve into a band of separate islands on an elliptic band. It is reasonable to expect that the orbit determined by the initial condition has a period equal to the number of islands in the band. Numerical study is consistent with this expectation. The center of each ellipse in the band is a periodic orbit of length equal to the number of islands in the band. For some initial conditions we have a

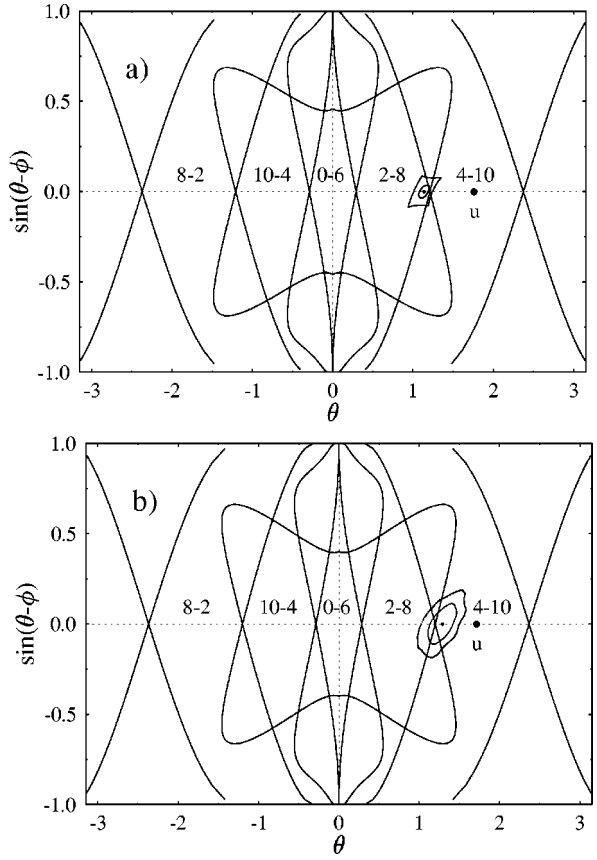

FIG. 6. Phase space partitioning for the initial conditions of length-2 orbits in the periodic Lorentz gas. For example, those initial conditions within the region labeled 2-8 produce a trajectory for which the first two symbols are 2 then 8. For $\epsilon = 2.25$ (a) the elliptic fixed point lies inside the 2-8 region and is thus pruned by scatterer number 2. The elliptic region that surrounds this point consists of a series of ellipses of increasing radius (determined by the initial point) ending in a curvilinear four sided boundary. As a trajectory beginning on the boundary, in general, visits many points on the boundary, the fact that some of the boundary is pruned by scatterer 2 effectively removes all elliptic orbits. The unstable periodic point of the 4-10 region is labeled u. For $\epsilon = 2.35$ (b) the elliptic fixed point is within the 4-10 partition so is physically realizable, and all ellipses surrounding that fixed point that lie wholly within the 4-10 partition are also physically realizable. For this value of the field, the boundary of the elliptic region is shaped like an irregular ellipse.

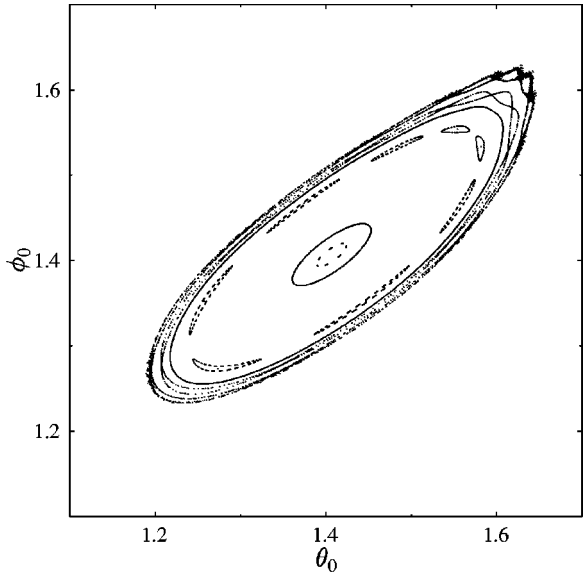

FIG. 7. Structure of the elliptic region with $d = 2.236$ and $\epsilon = 2.42$. Near the center the orbit consists of seven separate islands, while near the boundary the border consists of ten islands. Between the two limits the region is structured with bands of eight and nine islands sandwiched between ellipses. In the case of the eight island band structure, the eight points composing a length-16 periodic orbit are visible at the center of each island. On the border, trajectories escape from the elliptic region from the hyperbolic points created where the islands join.

band structure in which the separate islands begin to join at their edges. The joins are hyperbolic points in the phase space, so they produce elliptic and hyperbolic points in equal numbers. Numerical study showed that for certain appropriate initial conditions even the individual ellipses in the band can be split into a number of separate rings. This clearly indicates the self-similarity and fractal structure of the orbits in the elliptic region. The number of rings in the band increases as the initial condition departs further from the center. But between these bands the trajectory is confined to a single ellipse. The emergence of the bands with a greater number of rings continues until the initial conditions reach the border of the elliptic region. All of the above features closely resemble the behavior of resonant tori in Hamiltonian systems under a small perturbation [19]. In Fig. 7 the structure of the elliptic region at $\epsilon = 2.42$ and $d = 2.236$ is displayed. For initial conditions near the elliptic fixed point, the trajectory of the collision point orbits the fixed point. The band structure with the least number of islands (seven) appears near the center. For the next step the trajectory is confined to an ellipse, outside of which is the band with 8 islands. Periodic orbits of length eight are visible at the center of each island. A single ellipse emerges again for next stage. Further departure from the center causes the emergence of a band with nine islands that are joined. The outermost band is the border of the elliptic region and has ten islands. As mentioned before, the joins are hyperbolic points, so that the trajectory escapes from the neighborhood of the elliptic region most rapidly near these points. The trajectory steps from island to island in a clockwise direction. The eigenvalues for the mapping depend upon the initial condition and vary from island to island, with approximately half of the islands making a complex contribution to the eigenvalues and the rest a real contribution to the eigenvalues. However, for at least one of the islands, the initial conditions within the same island can make either a complex or imaginary contribution to the eigenvalues, depending upon the initial condition. Thus the stability varies from point to point on the ten islands, but the average of the product of the modulii of the eigenvalues is equal to unity, so the Lyapunov exponent is equal to zero.

IV. DISCUSSION AND CONCLUSIONS

In summary, we have determined the range of parameters for which the random Lorentz gas can have a nonergodic component surrounding the length-2 periodic orbits. There exists a maximum value for the separation of the disks d, above which length-2 orbits are hyperbolic for the whole

possible range of fields. On the other hand, the existence of the elliptic region is possible only for fields $\epsilon > 1.0$. Using stability analysis we found that the length-2 periodic orbits can be either hyperbolic or elliptic. The initial hyperbolic and elliptic regions have been reported previously, but the existence of a small range of fields for which real negative eigenvalues occur (and hence a return to hyperbolic orbits) has not been observed. The hyperbolic orbits appear as single points in the phase space, whereas the elliptic region occupies a region of nonzero measure. In the elliptic region the initial state vector rotates and dilates due to the complex eigenvalues. This is usually observed in area preserving maps. Extensive numerical study reveals a highly complex structure of the elliptic region. The emergence of the hyperbolic points at the junctions of islands signals chaos within the orbit (hyperbolic instability) and eventually leads to the breakdown of elliptic behavior and the boundary between the elliptic and chaotic regions. As the initial conditions depart from the center, elliptic orbits experience subsequent changes in structure, closely resembling the resonant tori in Hamiltonian systems, splitting into separate ellipses, confinement to a single ellipse, and again splitting into a greater number of islands. Even the individual islands in the band split into smaller islands, manifesting self-similarity, which may be the sign of an underlying fractal-like structure.

ACKNOWLEDGMENT

One of us (H.O.) gratefully acknowledges the AUSAID for financial support.

[1] P. Cvitanovic, P. Gaspard, and T. Schreiber, Chaos **2**, 85 (1992).
[2] W.N. Vance, Phys. Rev. Lett. **69**, 1356 (1992).
[3] J. Lloyd, M. Niemeyer, L. Rondoni, and G.P. Morriss, Chaos **5**, 536 (1995).
[4] A. Baranyai, D.J. Evans, and E.G.D. Cohen, J. Stat. Phys. **70**, 1085 (1993).
[5] N.I. Chernov, G.L. Eyink, J.L. Lebowitz, and Ya.G. Sinai, Commun. Math. Phys. **154**, 569 (1993).
[6] C.P. Dettmann and G.P. Morriss, Phys. Rev. E **54**, 4782 (1996).
[7] C.P. Dettmann, G.P. Morriss, and L. Rondoni, Chaos Solitons and Fractals **8**, 783 (1997).
[8] C.P. Dettmann, G.P. Morriss, and L. Rondoni, Physica A **240**, 87 (1997).
[9] D.J. Evans, E.G.D. Cohen, and G.P. Morriss, Phys. Rev. A **42**, 5990 (1990).
[10] D.J. Evans, E.G.D. Cohen, and G.P. Morriss, Phys. Rev. Lett. **71**, 2401 (1993).
[11] D.J. Evans and G.P. Morriss, *Statistical Mechanics of Non-Equilibrium Fluids* (Academic Press, London, 1990).
[12] G. Gallavotti and E.G.D. Cohen, J. Stat. Phys. **84**, 899 (1995), Phys. Rev. Lett. **74**, 2694 (1995).
[13] J. Lloyd, L. Rondoni, and G.P. Morriss, Phys. Rev. E **50**, 3416 (1994).
[14] H. van Beijeren, J.R. Dorfman, E.G.D. Cohen, H.A. Posch, and Ch. Dellago, Phys. Rev. Lett. **77**, 1974 (1996).
[15] A. Latz, H. van Beijeren, and J.R. Dorfman, Phys. Rev. Lett. **78**, 207 (1997); H. van Beijeren, A. Latz, and J.R. Dorfman, Phys. Rev. E **57**, 4077 (1998).
[16] Ch. Dellago and H.A. Posch, Phys. Rev. Lett. **78**, 211 (1997).
[17] H. van Beijeren (private communication).
[18] T. Gilbert, C.D. Ferguson, and J.R. Dorfman, Phys. Rev. E **59**, 364 (1999).
[19] Edward Ott, *Chaos in Dynamical Systems* (Cambridge University Press, Cambridge, 1994).
[20] C.P. Dettmann and G.P. Morriss, Phys. Rev. E **54**, 2495 (1996).
[21] P. Gaspard, *Chaos, Scattering, and Statistical Mechanics* (Cambridge University Press, Cambridge, 1998).